

# Low-Loss Off-Axis Feeds for Symmetric Dual-Reflector Antennas

T. Veruttipong, V. Galindo-Israel, and W. Imbriale  
Radio Frequency and Microwave Subsystem Section

*Circularly symmetric, dual-reflector, high-gain antenna systems often require feeds placed off the system's axis because of the need for multiple feeds to use the reflector antenna. Also, the constraint requiring the hyperboloid or shaped subreflector to remain circularly symmetric is sometimes added. In a Cassegrainian system, the subreflector and feed may be rotated off-axis around the paraboloid focus and retain main reflector focusing. However, substantial spillover results in considerable noise with a high-gain/low-noise temperature system. In a shaped system, the tilt of the shaped subreflector and feed together results in substantial defocusing as well as spillover noise. If the subreflector is tilted approximately one-half the angle of the feed tilt in either the Cassegrainian or the dual-shaped reflector antenna, it is found that spillover and noise are substantially reduced with tolerable defocusing. An extensive numerical analysis of these effects was conducted to determine the characteristics of a planned 70-meter, dual-shaped reflector versus Cassegrainian antenna and to gain some understanding of the cause of the observed effects.*

## I. Introduction

In large ground antenna systems, it is often necessary to use multiple feeds for the same main reflector. Thus, a number of feeds can be tilted off the axis of the symmetric main reflector, each illuminating a tilted subreflector, often the same subreflector that is rotated into position for a given feed. This type of antenna system is shown in Fig. 1.

In some systems, such as the JPL 70-meter upgrade of the 64-meter antenna, the subreflector diameter can be more than 200 wavelengths at 8.45 GHz. A considerable cost savings is

possible if a circularly symmetric subreflector is used in place of an asymmetric offset subreflector. This is especially true for shaped reflectors (Refs. 1, 2, 3) that have no larger "parent" circularly symmetric reflector from which they could be cut. A circularly symmetric subreflector, if tilted, can also be useful for a feed located on the axis of the symmetric main reflector. This would result in "best" or "reference" performance, given the ability to "retilt" the otherwise tilted subreflector.

In the study of the off-axis-fed antenna system, the tilt angle of the feed relative to the tilt angle of the subreflector

was varied. The absolute angle of the tilt was also varied. These tilt angles for the feed ( $\alpha$ ) and for the subreflector ( $\beta$ ) are shown in Fig. 2.

The actual point of rotation of the feed and subreflector depends upon the type of reflector design used. For a Cassegrainian (parabola/hyperbola) system, the obvious choice for a rotation point is the paraboloid focus. For a dual-shaped reflector system, the choice is not obvious. The "optimum" choice for the shaped reflectors is discussed later.

In either case, when large (in wavelengths) reflectors are used, the off-axis displacements of the feeds may be many tens of wavelengths. Consideration will be given to the characteristics of a 70-meter dual-shaped reflector antenna that is an upgrade of a National Aeronautics and Space Administration/Deep Space Network (NASA/DSN) 64-meter design with off-axis feeds (see Fig. 2).

## II. Gain vs Off-Axis Rotation

There are two types of off-axis rotations of the feed and subreflector. In one case,  $\beta = \alpha$ : that is, the subreflector and feed are rotated by the same angle. For the Cassegrainian system, note that, in this case, the phase on the main reflector remains correct except where the main reflector becomes under-illuminated.

In a second case,  $\beta = \alpha/2$ . For this choice of  $\beta$ , we find that the main reflector remains neither under- nor over-illuminated. However, it is clear that a phase error is introduced for the Cassegrainian system. The significance of the proper amplitude illumination of the main reflector is that spillover past the main reflector results in a large receiving noise caused by the relatively hot earth surface beyond the main reflector. In the case when  $\beta = \alpha/2$ , the feed is always pointed toward the center of the subreflector.

The geometry and dimensions for the Cassegrainian system under study are shown in Fig. 3. An experimental corrugated feed horn was used for the dual-shaped reflector antenna geometry, shown in Fig. 4. The overall dimensions of the two antenna systems were kept approximately the same. The Cassegrainian subreflector was illuminated with a -10 dB taper at the edge of the subreflector.

The dual-shaped subreflector was illuminated with a -16 dB taper at the edge of the subreflector. The dual shaping was chosen for maximum gain. There was a small taper allowed near the edge of the main reflector. A slight extension of the main reflector beyond the geometric optics edge was introduced to reduce the noise temperature increase that normally comes from the tapering edge of the subreflector scattered

pattern. The subreflector was synthesized with a vertex plate blended into the synthesis (Ref. 1).

As a function of  $\alpha$ , the Cassegrainian system maintains a better gain curve than the shaped reflector antenna for  $\beta = \alpha$  (except for noise considerations). The dual-shaped reflector system maintains a significantly better gain curve than the Cassegrainian for  $\beta = \alpha/2$  provided that an optimum rotation point is chosen).

The gain versus  $\alpha$ -angle curves for the 70-meter designs are shown in Fig. 5 for the Cassegrainian and in Fig. 6 for the dual-shaped reflector systems.

The gain versus  $\alpha$  curve for  $\beta = \alpha$  in Fig. 5 is relatively flat, although the noise temperature increases with  $\alpha$ . The principal cause of a loss in gain is reduced illumination on one side of the main reflector (discussed in detail later). This reduction could be eliminated by choosing an offset asymmetric hyperboloid. However, the offset asymmetric subreflector can be used for only one  $\alpha$  angle and is more costly. The  $\beta = \alpha/2$  gain curve for the Cassegrainian antenna drops off rapidly with increasing  $\alpha$  because of an increasing aperture phase error. In this case, however, the illumination amplitude across the main reflector aperture has considerably less spillover and, therefore, considerably less noise is collected. Note also that for the  $\beta = \alpha$  case, there is no beam-pointing shift. The beam points in the  $\theta = 0$  direction for all  $\alpha$ . For the case with  $\beta = \alpha/2$ , there is an approximately linear shift of beam-pointing direction, as indicated in Fig. 5.

The gain versus  $\alpha$  results for the dual-shaped reflector are shown in Fig. 6. For  $\alpha = 0$ , the gain of the dual-shaped reflector is about 0.75 dB higher than for the Cassegrainian system. The relative aperture efficiencies (spillover and depolarization accounted for) are 80.5% for the Cassegrainian and 96.5% for the dual-shaped system (in both cases for  $\alpha = 0^\circ$ ).

The gain versus  $\alpha$  angle results for the dual-shaped antenna show that the performance for the case  $\beta = \alpha$  degrades rapidly and badly because of the introduction of both a phase and an amplitude error in the main reflector aperture distribution by the rotation of the feed and subreflector as a unit. The degradation in gain caused by the under-illumination of amplitude but is greater here than for the Cassegrainian antenna because the object illumination function resulting from dual shaping is nearly uniform.

When the shaped subreflector is rotated by the angle  $\beta = \alpha/2$  around the appropriate point of rotation, the results in gain versus  $\alpha$  angle are comparable to the Cassegrainian gain versus  $\alpha$  angle results for the  $\beta = \alpha$  case. Note that the shaped reflector system has the advantage over the Cassegrainian of a

lower noise amplitude distribution. Further explanation for this result will follow in the next section.

The actual frequency for these computations was 8.45 GHz. The radius of the main reflector was taken as 986.3 wavelengths. The computations were greatly facilitated by the use of a GTD analysis of the subreflector scattered field and a Jacobi-Bessel analysis (Refs. 4, 5, 6) of the main reflector scattered field. Various global and local interpolation methods (Ref. 7) were employed to analyze the shaped subreflector and main reflector.

A relevant question at this point is: Why is  $\beta = \alpha/2$  an "optimum" value of  $\beta$  as opposed to some other fractional portion of  $\alpha$ ? It does turn out that at  $\beta \cong \alpha/2$ , the amplitude distribution on the main reflector has minimum under-illumination. Figures 7 through 9 show the gain of Cassegrainian and dual-shaped reflector antennas as a function of the  $\beta$ -angle (tilt angle of the subreflector) with the  $\alpha$ -angle (tilt angle of the feed) fixed.

For the Cassegrain antenna (with  $\alpha$  fixed at  $10.52^\circ$ ), note that the gain peaks when  $\beta = \alpha$ . This is expected because the aperture phase is correct at  $\beta = \alpha$ , and the phase is more critical than the amplitude. For the dual-shaped reflectors, the result is quite different. In this case, the gain peaks at approximately  $\beta = \alpha/2$  for both  $\alpha = 10.52^\circ$  and  $\alpha = 4.482^\circ$  (see Figs. 8 and 9). Again, the phase, as well as the amplitude, is optimum. As noted later (for the shaped reflectors), the phase function is optimum at approximately  $\beta = \alpha/2$  when the "best" rotation point is chosen. This is related to the fact that the field scattered from the subreflector has an extended set of two caustic surfaces as opposed to the single caustic point for the Cassegrainian antenna. These caustic surfaces are discussed later.

All the preceding results were for circularly symmetric subreflectors, shaped and conic (Table 1). For the case  $\beta = \alpha/2$ , the Cassegrainian system suffers a phase error in the main reflector aperture. For the case  $\beta = \alpha$ , the Cassegrainian system suffers an amplitude distortion with subsequent increased receiver noise. Both of these deficiencies can be removed with an asymmetric hyperboloid (in the plane of rotation of the feed and subreflector). For comparison, results with an asymmetric hyperboloid subreflector are shown in Table 1. For  $\alpha$  less than about  $6^\circ$ , there is only about 0.1 dB difference between the various cases (see Fig. 5). Although the asymmetric reflector gives marginally better performance, the  $\beta = \alpha/2$  case gives equivalent results with a less expensive symmetric hyperboloid. Note that when diffraction from the subreflector is ignored, the gain is increased by 0.1 dB, a direct measure of spillover loss for the Cassegrain (usually much higher for electrically smaller antennas).

A final point for consideration in this section is the determination of the point of rotation of the subreflector and feed for the dual-shaped reflector system. Because an incoming plane wave reflected from the shaped main reflector will not come to a virtual point focus, the precise optimum point of rotation is not immediately clear. In Fig. 10, all rays do intersect along a caustic line behind the subreflector (in the non-rotated position). For a Cassegrain antenna, this line degenerates into a point. Actually, this caustic arises from the curvature out of the plane of the paper. It would seem that an "optimum" point of rotation for the shaped system would lie within the limits of this caustic line.

The position may be weighted along the caustic by plotting the caustic intersection point versus position ( $\rho$ ) along a radius of the main reflector (also shown in Fig. 10). For the Cassegrain, all rays intersect at a fixed  $z$  position, which is the focus. For the shaped system, different radial positions along the main reflector correspond to different positions of intersection along the  $z$ -axis. Because the main reflector aperture distribution is nearly uniform, an accordingly weighted mean  $z$  position may be chosen as an optimum point of rotation.

A more direct method of choosing the optimum point is observed in Fig. 11. The feed lateral displacement is fixed at  $\Delta X$ ; then the subreflector is rotated to the position  $\beta = \alpha/2$  with different points,  $F'$ , of rotation. It is known that  $\beta = \alpha/2$  is an approximately optimum ratio between  $\alpha$  and  $\beta$  for the shaped reflectors. The optimum position,  $F'$ , of rotation is in the vicinity of the weighted curve of Fig. 10.

Figure 10 shows that the main reflector line caustic  $z$ -position doubles back on itself near  $\rho = 9.75 \lambda$ . Thus, there is an additional intersection of rays off the  $z$ -axis. This intersection is the caustic from curvature of the field in the plane.

### III. Far-Field Patterns and Reflector Currents

In this section, the far-field patterns of both the Cassegrainian and the dual-shaped 70-meter antennas are presented as a function of the  $\alpha$  and  $\beta$  angles ( $\beta = \alpha$  and  $\beta = \alpha/2$  cases). The main reflector current distributions are also reviewed to obtain some insight into the characteristics of these antennas with  $\alpha$  and  $\beta$  angles of feed and subreflector rotation.

Figure 12 shows the far-field patterns of the 70-meter shaped and Cassegrain systems with  $\alpha = \beta = 0$ , the concentric case. In addition to the vertex plate on the subreflector of the shaped reflectors, the shaped main reflector also has an extension that serves as a noise shield; i.e., it shields the feed from the average 240 K ground noise in that critical area of sharp energy drop-off near the main reflector edge. The shaped sys-

tem attains about 96.6% efficiency, whereas the Cassegrainian system attains about 70.2% efficiency (with a  $-10$  dB feed taper and blockage not accounted for). Spillover and cross-polarization losses are accounted for in these computations.

The pattern degradation of the Cassegrainian system with an increasing  $\alpha$  angle is not great because the main reflector currents remain properly in phase over most of the reflector, except the under-illuminated portion. The degradation is, however, more apparent for the  $\beta = \alpha/2$  case. This is illustrated in the patterns of Fig. 13. Note that the vertical gain scale is shifted for each pattern; the change in gain between patterns is noted next to each pattern. Of special interest is the actual beam-pointing direction for each pattern, noted next to the pattern by  $\theta_B$ . With a 3-dB beamwidth of less than  $0.05^\circ$ , the beam shift from the concentric  $\alpha = \beta = 0^\circ$  case is many beamwidths.

The pattern degradation is very great for the shaped reflector antenna when  $\alpha = \beta$ . This is clear because even when the subreflector and feed are rotated about an optimum point on the caustic (see Fig. 10), there is substantial phase defocusing for the  $\alpha = \beta$  case. However, for the  $\beta = \alpha/2$  case, the defocusing is substantially reduced, and the beam is shifted with considerably less loss in gain and degradation in pattern structure. This is shown in Fig. 14.

Of special interest in the far field is what occurs to the phase and the amplitude monopulse patterns when the feed and subreflector are rotated so that  $\beta = \alpha/2$ . To observe this effect with the Cassegrainian antenna, a "synthetic" feed monopulse pattern was used. This pattern, as well as the sum pattern for the Cassegrainian feed, is shown in Fig. 15. The effect of the asymmetry for the case with  $\alpha = 4.52^\circ$  is shown in Fig. 16. Although the "null" of the amplitude pattern is not as deep as for the  $\alpha = 0^\circ$  case and the phase shift of  $180^\circ$  at the sum pattern maxima is not as sharp, the monopulse pattern might be usable.

Before investigating the currents on the main reflector, it is of interest to look at the  $\alpha = 0^\circ$  concentric scattered fields from the shaped subreflector and the hyperboloid subreflector. These are shown in Fig. 17. The patterns are for the near fields in the vicinity of the main reflectors. It is apparent for such large subreflectors (approximately  $200\lambda$ ) that the vertex plate is extremely effective. Furthermore, the optical projection approximation accounting for subreflector blockage is also accurate. Also apparent is the relatively precise secant squared behavior (for high gain) achieved by the shaped reflector system.

The current distributions on the main reflectors in the plane of feed and subreflector rotation are shown in Figs. 18

through 21. Both amplitude and phase are shown for the Cassegrainian and shaped systems at  $\beta = \alpha$  and  $\beta = \alpha/2$ . The object is to gain some further insight into what is occurring within the reflector systems that causes the result in gains and the far-field patterns that has already been observed.

Figure 18 shows the paraboloid currents as a function of parameter  $\alpha$  when  $\beta = \alpha$ . (The curves are displaced vertically so that their relative functional characteristics are easily compared.) Note that the phase curves remain flat except where under-illumination of the paraboloid occurs (to the left). The under-illumination is evident in the amplitude curves. The under-illumination to the left is matched by an over-illumination to the right. This over-illumination increases the noise of the antenna substantially for a ground system antenna looking toward zenith. The over-illumination receives an average of approximately 240 K ground radiation, as compared to an over-illuminated space antenna which would receive approximately 2.7 K galactic noise. This is one of the principal motivations for using rotation angles  $\beta = \alpha/2$  for the feed and subreflector of a ground Cassegrainian antenna.

When  $\beta = \alpha/2$ , the over- and under-illumination of the paraboloid are reduced substantially. This is observed in Fig. 19 over a wide range of  $\alpha$  from  $\alpha = 0^\circ$  to  $\alpha = 14.52^\circ$ . The penalty for this well-illuminated paraboloid in amplitude is a phase error illumination, which is also observed in Fig. 19. A linear beam-shift phase term has been subtracted from the phase curves so that what is depicted as displaced from a flat curve is a phase error. As observed in Fig. 3, the phase error is not significant (relative to the  $\alpha = \beta$  case) until  $\alpha$  is greater than  $6^\circ$ .

For the dual-shaped reflectors, the situation is very different. When  $\alpha = \beta$  is maintained and  $\alpha$  is increased, not only does a poorly illuminated main reflector suffer in amplitude, but it also displays substantial phase error. This is shown in Fig. 20. Also, the amplitude over- and under-illumination effects are more severe here than for the Cassegrainian antenna because the illumination amplitude is nearly uniform or flat. This is a result of the secant-squared subreflector scattered pattern (see Fig. 17).

As a result, it is fortuitous that rotating the subreflector with  $\beta = \alpha/2$  gives such excellent results for the dual-shaped reflector antenna. The current distributions for this situation as a function of the parameter  $\alpha$  are shown in Fig. 21. The phase curves are relatively flat for a large range of  $\alpha$  (after subtraction of the appropriate linear beam-shift phase). The resulting gain curve as a function of  $\alpha$  (see Fig. 4) is comparable to that obtained for the Cassegrainian curve, although higher in value as a result of the shaping.

The main reflector current curves clarify what is occurring to the amplitude distribution on the main reflectors when  $\alpha = \beta$  and when  $\beta = \alpha/2$ . It is clear that when  $\alpha = \beta$ , a large noise temperature can occur for ground system antennas looking upward, and that setting  $\beta$  equal to  $\alpha/2$  will largely alleviate this problem for both the Cassegrainian and the dual-shaped reflector systems.

It is also evident why the main reflector current phase is excellent (nearly flat) for the Cassegrainian antenna when  $\beta = \alpha$ . However, an understanding of why the main reflector current phase curves are as flat as they are for  $\beta = \alpha/2$  requires further investigation.

#### IV. Caustic Characteristics of the Subreflector Scattered Fields

Further insight into why the shaped main reflector phase current distributions are as flat as observed for  $\beta = \alpha/2$  (see Fig. 21) can be obtained by studying the caustic surfaces of the geometrical optics fields scattered from the subreflector.

In the plane of rotation of the feed and subreflector, the Gaussian curvature matrix is diagonal (by symmetry), and a line caustic for the radius of curvature out of the plane  $-R_o$  can be observed; another line caustic for the radius of curvature is parallel to the plane  $-R_p$ .

A set of the above line caustics (for different  $\alpha$ ) can be plotted relative to the subreflector and relative to the main reflector. When the caustic lines relative to the main reflector for  $\alpha = 0^\circ$  and for  $\alpha > 0^\circ$  are plotted, a relative comparison can be made of how much the  $\alpha > 0^\circ$  caustic lines deviate from the ideal  $\alpha = 0^\circ$  caustic line. This deviation is a visual measure of the phase distortion that is observed on the main reflector for  $\alpha > 0^\circ$ .

For the Cassegrainian antenna and  $\alpha = \beta$ , both caustic lines degenerate into a point for all  $\alpha$ . This point is the focal point of the hyperboloid and paraboloid. When  $\beta = \alpha/2$ , caustic lines are obtained as shown in Fig. 22. In Fig. 22, the caustic lines are plotted relative to the subreflector for all  $\alpha$ . To observe the caustics relative to the main reflector, each caustic must be rotated about the rotation point (focal point) by the value of  $\alpha$ .

In Fig. 23, the same caustic lines are observed in an enlarged diagram. The rays emanating from the caustics are tangent to the caustic surfaces. For the  $R_o$  curves, the rays are tangent to a cusp of the surface in the plane of the paper. The rays depicted in the top diagram are all directed toward one end of the main reflector. However, because of the rotation of the feed and subreflector assembly, the main reflector is rotated

for each caustic line by  $\alpha$ ; i.e., the curves are plotted relative to the subreflector. (The rays appear parallel, but they are not.) The lower diagram of Fig. 23 shows rays distributed to all parts (in the plane) of the main reflector.

The computation and plotting of the caustics were performed during a geometrical optics analysis of the field scattered by the subreflector. In this analysis, two radii of curvature were computed by the equations shown in Fig. 24. These radii of curvature,  $R_1$  and  $R_2$ , relate directly to  $R_o$  and  $R_p$ , but not uniquely or consistently (a branch choice must be made). In order to relate  $R_1$  and  $R_2$  to  $R_o$  and  $R_p$  through the scattered field ( $\alpha$  fixed), the expedient of making the subreflector cylindrical is used as indicated in the lower diagram of Fig. 24. This immediately makes  $R_o$  extremely large (less than infinity because of the spherical wave incident upon the subreflector from the feed). The curvature  $R_p$  is not changed by this artifice. An appropriate match of  $R_1$  to  $R_o$  or  $R_p$  and of  $R_2$  to  $R_p$  or  $R_o$  is made accordingly.

The principal motive for examining the caustic lines is to further understand the phase characteristics of the dual-shaped reflectors. The caustic lines for the shaped subreflector scattered fields are very different from those encountered for the field scattered by the hyperboloid. This is apparently true for offset as well as circularly symmetric-shaped reflectors.

Figure 25 shows the caustic lines for the field scattered by a focused feed from an offset shaped subreflector (Refs. 8, 9). Note that the vertical scale for the inset diagram is many times greater than the scale for the full diagram; thus, the  $R_p$  caustic is extremely large. The wavefront scattered from the subreflector is nearly planar in the plane of the diagram and near the extremities. It is also now clear that the caustic line discussed earlier and displayed in Fig. 10 is an  $R_o$  caustic or is due to curvature orthogonal to the plane of the diagram.

The  $R_p$  caustic lines for different  $\alpha$ , with  $\beta = \alpha/2$ , are displayed in Fig. 26 for the 70-meter shaped reflectors. They are similar in character to the offset-shaped case of Fig. 25, though this case is distinct from that of the Cassegrainian system. In Fig. 26, the  $R_p$  caustics are shown with respect to the subreflector. In Fig. 27, the same  $R_p$  caustic lines are plotted with respect to the main shaped reflector. The subreflector is appropriately located only for the  $\alpha = 0^\circ$  case. The main reflector is to the left, fixed for all  $\alpha$  values. Note that the caustic lines for various  $\alpha$  all lie nearly parallel, especially for  $\alpha < 6^\circ$ . Thus, the phase of the geometrical optic field incident upon the main reflector will be relatively unchanged for  $\beta = \alpha/2$ . This phase compensation occurs in addition to very little over- and under-illumination of the main reflector. Therefore, the shaped reflector performance with  $\beta = \alpha/2$  is very good.

In Fig. 28, observe the  $R_o$  (curvature orthogonal to the diagram) caustic characteristics for various  $\alpha$  for the same 70-meter shaped reflector system. Note again that with respect to the main reflector (right-hand diagram), the caustic lines become much closer. The enlarged diagrams of Fig. 29 show this more clearly.

## V. Conclusion

In a circularly symmetric, high-gain, dual-reflector antenna system, a very substantial off-axis feed displacement can be accommodated while retaining a circularly symmetric sub-reflector. This can be done with little gain or gain/noise temperature ( $G/T$ ) loss for both Cassegrainian and dual-shaped reflectors. In both cases (the Cassegrainian and the dual-shaped antennas), performance is substantially improved if the subreflector is rotated off-axis by an angle  $\beta$  that is one-half the angle of rotation of the feed,  $\alpha$ . This is imperative for the shaped reflectors because there is no unique phase center about which to rotate the subreflector and feed. However, to obtain an optimum  $G/T$  for the Cassegrain reflectors (as well as the shaped reflectors), maintaining  $\beta = \alpha/2$  is important. Although the main reflector phase distortion is kept fairly small, the relationship  $\beta = \alpha/2$  ensures very little spillover of energy past the main reflector into a hot (240 K) ground.

In the hypothetical Cassegrain system discussed in this article, no noise shield was used. Thus, the noise temperatures

shown as a function of  $\alpha$  (feed rotation angle about the Cassegrainian focal point), with  $\beta = \alpha/2$  or  $\beta = \alpha$ , are higher than can be obtained with a noise shield.

A typical good system (a DSN 64-meter antenna) may have a noise temperature distribution as shown in Table 2. If the dichroic and rear spillover noises are removed from the zenith elevation values of Table 2, about 14.6 K remains. The noise temperatures displayed in Fig. 30 can be added to this value as a function of  $\alpha$ , and  $G/T$  values can be obtained as a function of  $\alpha$  for the Cassegrainian system used herein for  $\beta = \alpha$  and for  $\beta = \alpha/2$ . This result is displayed in Fig. 31(a). Note in Fig. 31(a) that the  $G/T$  performance is superior for the  $\beta = \alpha/2$  case despite the phase error introduced by the  $\beta = \alpha/2$  value of the feed location. This is a direct result of the substantially flat and low noise temperature found for the  $\beta = \alpha/2$  case (see Fig. 30). The difference in the  $G/T$  curves in Fig. 31(a) would be even greater if a noise shield were built into the Cassegrainian design. The difference is slightly less if a less optimistic noise temperature for the system is assumed: i.e.,

$$T_{\text{system}} - T_{\text{antenna}} = 20 \text{ K}$$

The result, shown in Fig. 31(b), would apply for an antenna elevation angle below zenith.

## Acknowledgment

The concept of rotating a symmetric subreflector by one-half the feed offset angle to minimize the scan loss was originally proposed by Gerry Levy (Ref. 10) for a nonshaped Cassegrainian system. The authors wish to thank R. C. Clauss for providing both the funding, through the Advanced Systems Program, and the impetus to study the problem by insisting that it would also work for a shaped system.

## References

1. Galindo-Israel, V., and Mittra, R., Synthesis of Offset Dual-Shaped Reflectors with Arbitrary Control of Phase and Amplitude, *1977 URSI Symp. on Electromagnetic Theory, 20-24 June 1977*, pp. 7-10, International Scientific Radio Union, 1977.
2. Galindo-Israel, V., Mittra, R., and Cha, A., Aperture Amplitude and Phase Control of Offset Dual Reflectors, *IEEE Trans. Antennas Propagat.*, AP-27: 154-164, 1979.
3. Galindo, V., Design of Dual Reflector Antennas and Arbitrary Phase and Amplitude Distribution, *IEEE Proc. Int. Symp. Antennas and Propagat.*, Boulder, Colorado; also in *IEEE Trans. Antennas Propagat.*, AP-12: 403-408, 1963-1964.
4. Galindo-Israel, V., and Mittra, R., A New Series Representation for the Radiation Integral with Application to Reflector Antennas, *IEEE Trans. Antennas Propagat.*, 25:631-641, 1977.
5. Mittra, R., Rahmat-Samii, Y., Galindo-Israel, V., and Norman, R., An Efficient Technique for the Computation of Vector Secondary Patterns of Offset Paraboloid Reflectors, *IEEE Trans. Antennas Propagat.*, 27:294-304, 1979.
6. Rahmat-Samii, Y., and Galindo-Israel, V., Shaped Reflector Antenna Analysis Using the Jacobi-Bessel Series, *IEEE Trans. Antennas Propagat.*, 28:425-435, 1979.
7. Galindo-Israel, V., Imbriale, W., Rahmat-Samii, Y., and Veruttipong, T., Interpolation Methods for GTD Analysis of Shaped Reflectors, *TDA Progress Report 42-80*, pp. 62-67, Jet Propulsion Laboratory, Pasadena, Calif., 1984-1985.
8. Cha, A., Wideband Diffraction Improved Dual-Shaped Reflectors, *IEEE Trans. Antennas Propagat.*, AP-30: 173-176 (theoretical predictions herein subsequently totally verified experimentally).
9. Cha, A., Galindo-Israel, V., and Mittra, R., Efficient Design of Offset Dual-Shaped Reflectors for Antenna and Beam Waveguide Applications, *1979 Int. Symp. Digest, Antennas and Propagat., Vol. 1*, pp. 84-87, 79-CH1456-3 AP, IEEE, New York, 1979.
10. Levy, G. S., and Katow, M. S., Multi-feed Cone System for the Advanced Antenna Systems, *Space Prog. Summary 37-45 Vol. III*, pp. 48-50, Jet Propulsion Laboratory, Pasadena, Calif., 1967.

**Table 1. Cassegrain gains**

Configuration	Angle Case, deg	Gain, dBi
Concentric Cassegrain	$\beta = \alpha = 0$	74.90
Asymmetric Hyperboloid	$\beta = \alpha = 4.5165$	74.86
Asymmetric Hyperboloid (No Diffraction from Subreflector)	$\beta = \alpha = 4.5165$	74.96
Symmetric Hyperboloid	$\beta = \alpha = 4.5165$	74.71
Symmetric Hyperboloid	$\alpha = 4.5165 \left( \beta = \frac{\alpha}{2} \right)$	74.82

**Table 2. Noise for very good Cassegrainian system**

Noise Source	Zenith, $K$	30° Elevation
Amplifier	4.0	4.0
Waveguide at 300 K	4.7	4.7
Dichroic Surface	2.0	2.0
Galactic Noise	2.7	2.7
Atmosphere	2.6	5.2
Antenna		
Quadrapod	2.6	5.2
Rear Spillover	~0.4	~0.2
Total Noise	~17.0 K	~22.0 K

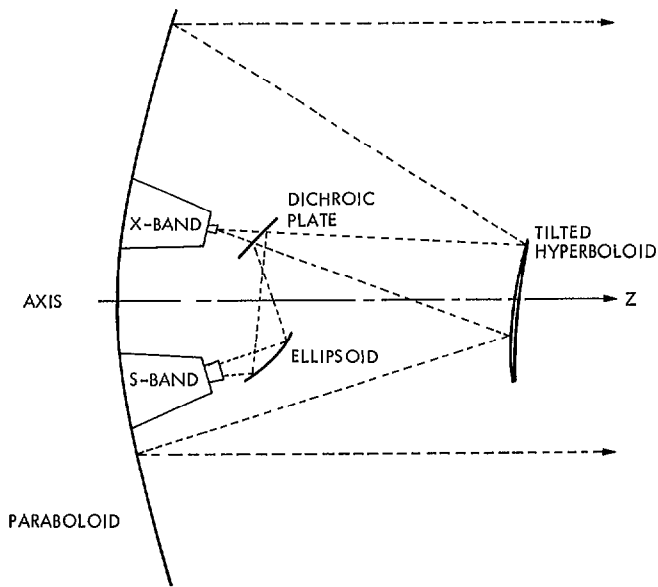


Fig. 1. Multiple feed, off-axis antenna system

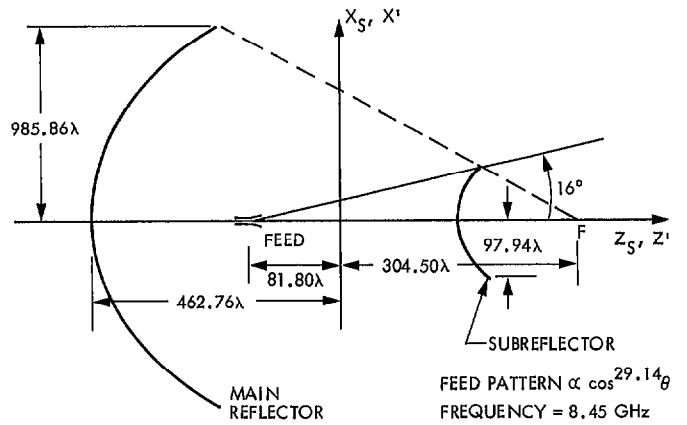


Fig. 3. Cassegrainian antenna geometry

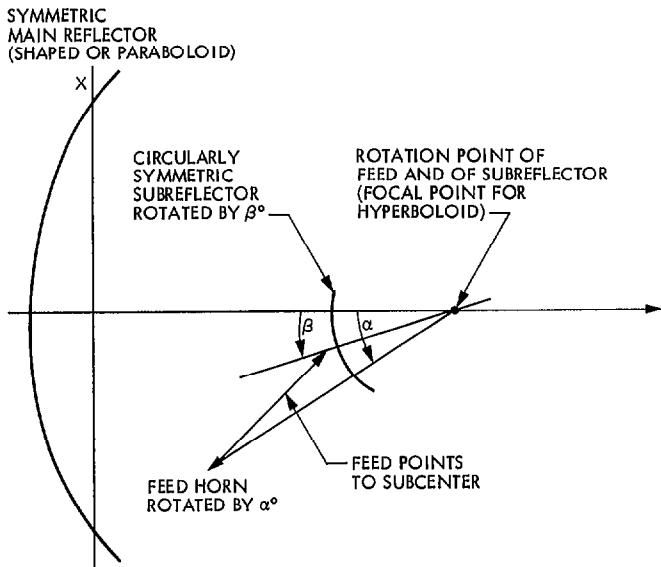


Fig. 2. Geometry for feed and subreflector rotation

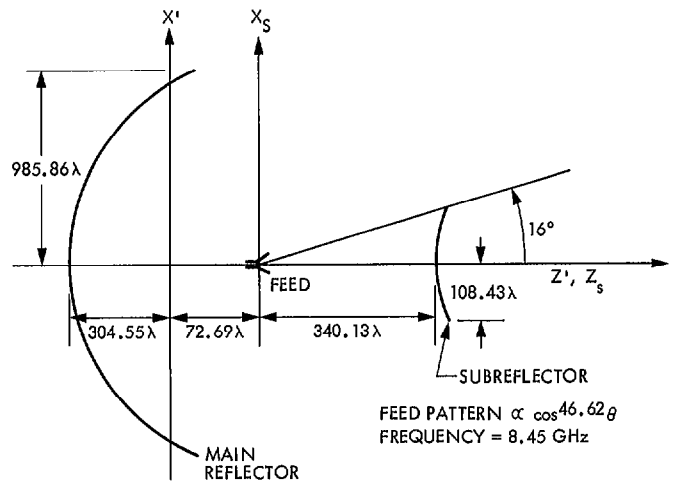


Fig. 4. Dual symmetric-shaped reflector antenna geometry

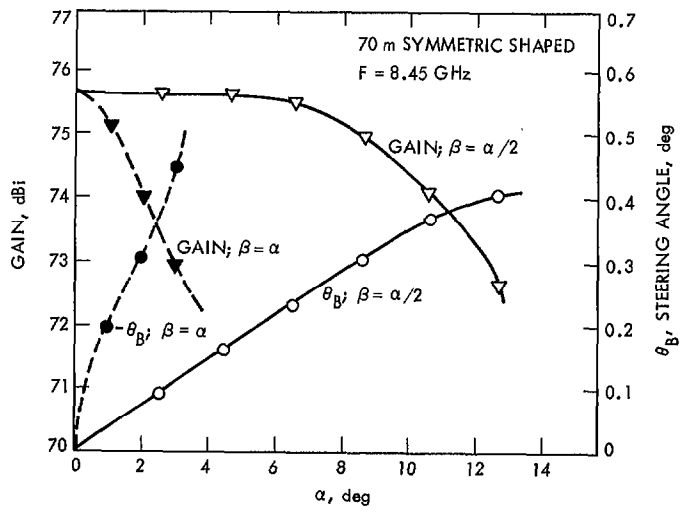
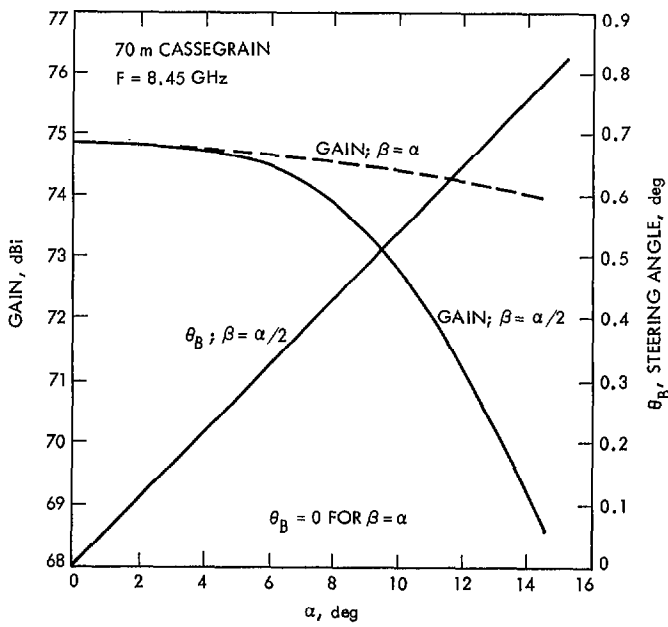
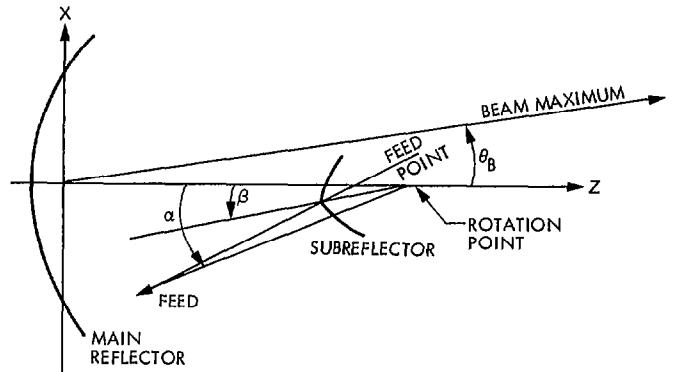
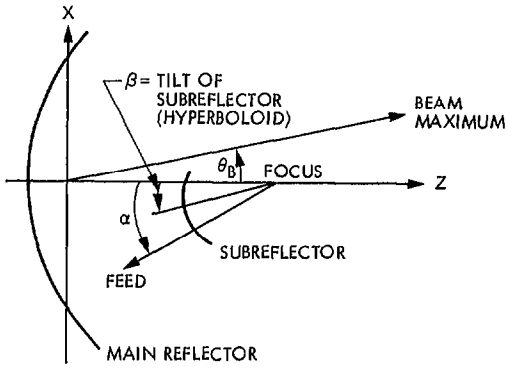


Fig. 5. Gain and steering angle vs feed horn rotated angle ( $\alpha$ ) for 70-m Cassegrainian antenna

Fig. 6. Gain and steering angle vs feed horn rotated angle ( $\alpha$ ) for 70-m dual symmetric-shaped reflector antenna

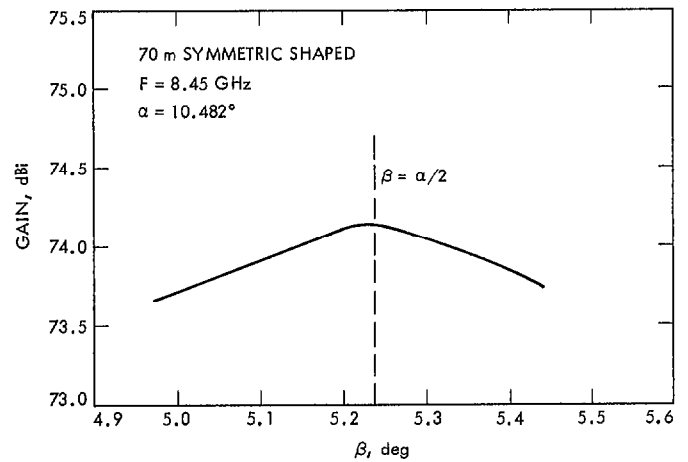
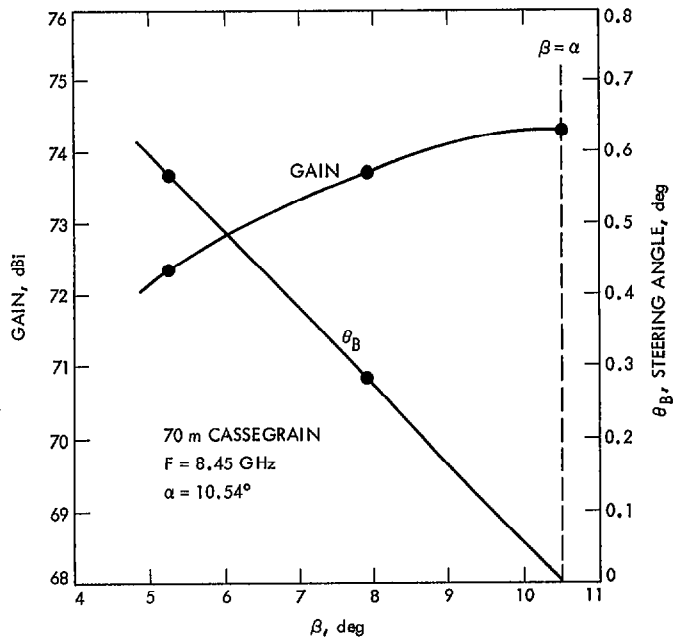
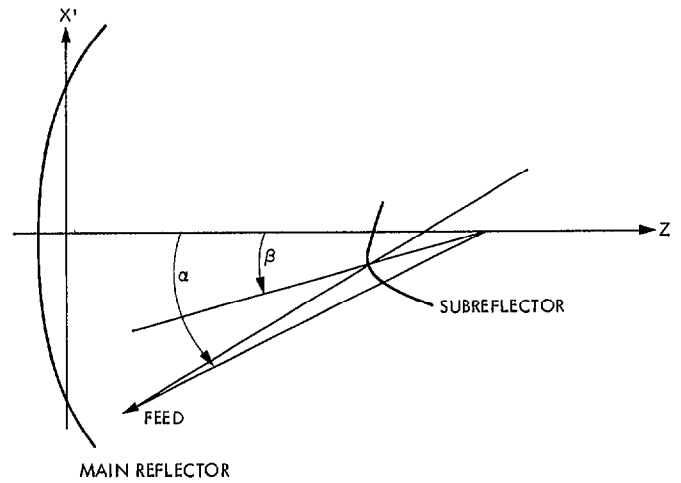
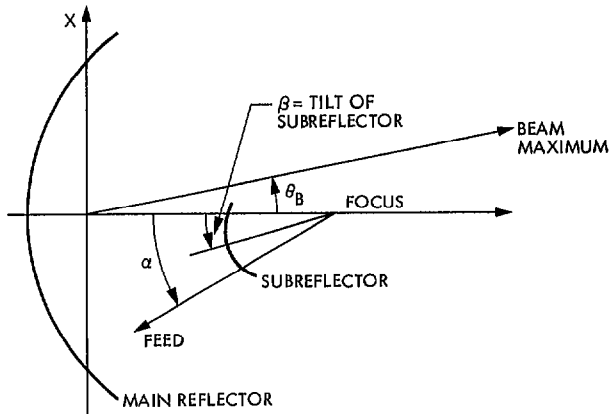
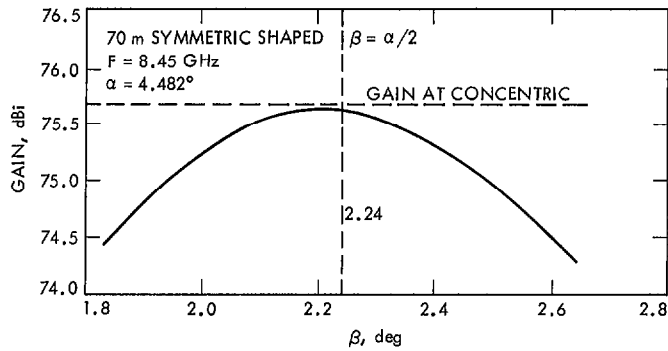
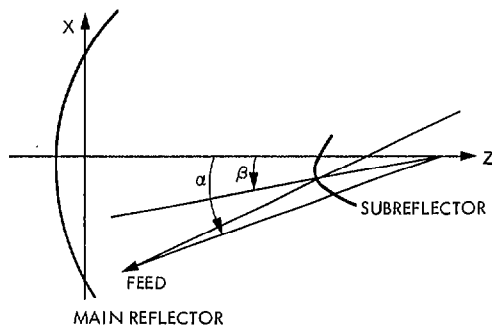
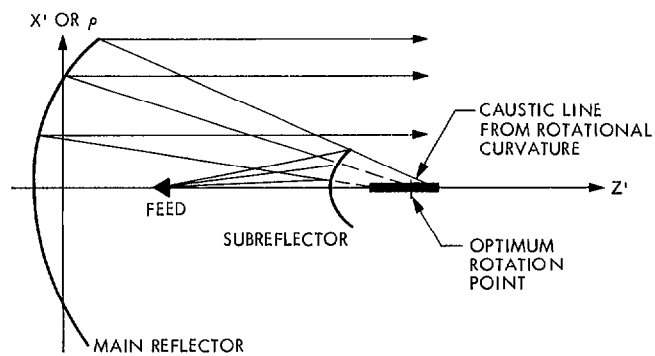
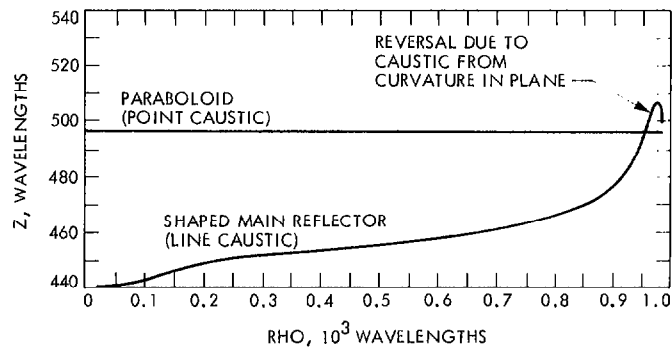


Fig. 7. Gain and steering angle vs tilt angle of subreflector ( $\beta$ ) for 70-m Cassegrainian antenna

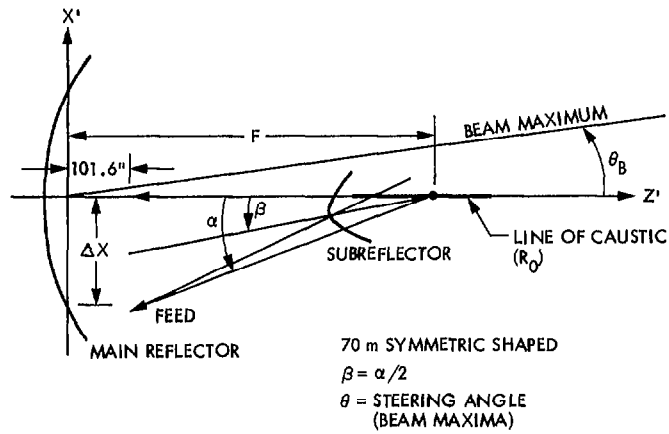
Fig. 8. Gain vs tilt angle of subreflector ( $\beta$ ) for 70-m dual symmetric-shaped reflector antenna with  $\alpha = 10.482^\circ$



**Fig. 9. Gain vs tilt angle of subreflector ( $\beta$ ) for 70-m dual symmetric-shaped reflector antenna with  $\alpha = 4.482^\circ$**



**Fig. 10. The z-caustic position due to rotational curvature (curvature out of plane)**



NO.	$\Delta X$ , in.	F, in.	$\alpha$ , deg	GAIN, dBi	$\theta_B$ , deg	
1	0.000	645.76	0.000	75.65	0.00	CONCENTRIC CASE
2	42.523	615.01	4.751	75.48	0.10	
3	42.523	645.76	4.482	75.58	0.16	
4	42.523	710.06	4.007	75.20	0.26	
5	42.523	641.60	4.517	75.59	0.15	BEST CASE

Fig. 11. The determination of the optimum point of rotation

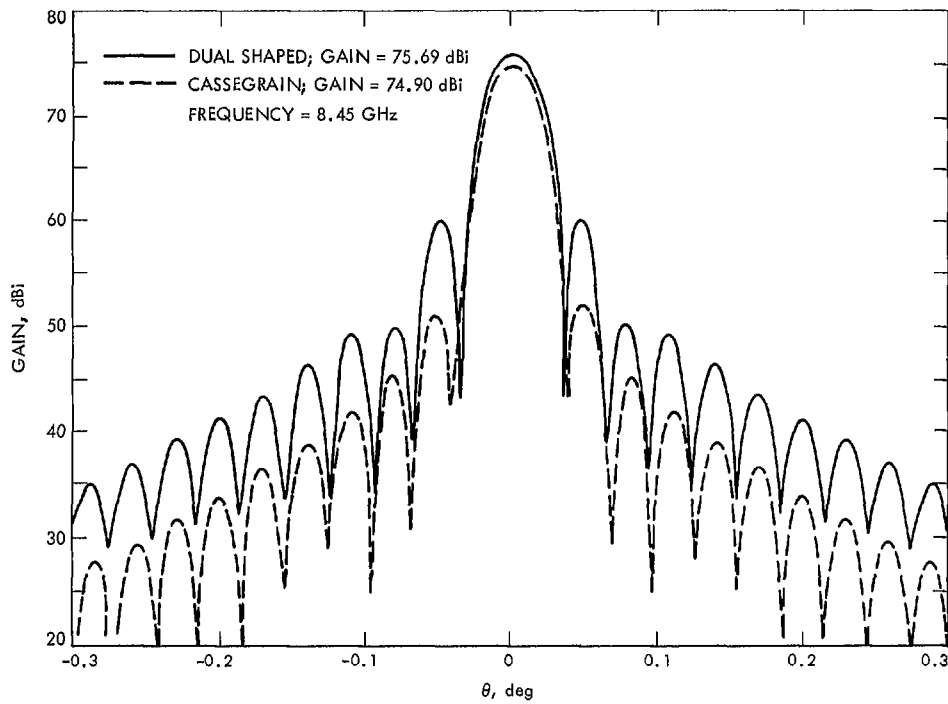


Fig. 12. Far-field gain patterns of the dual-shaped (with vertex plate) and Cassegrainian antennas with  $\alpha = \beta = 0^\circ$

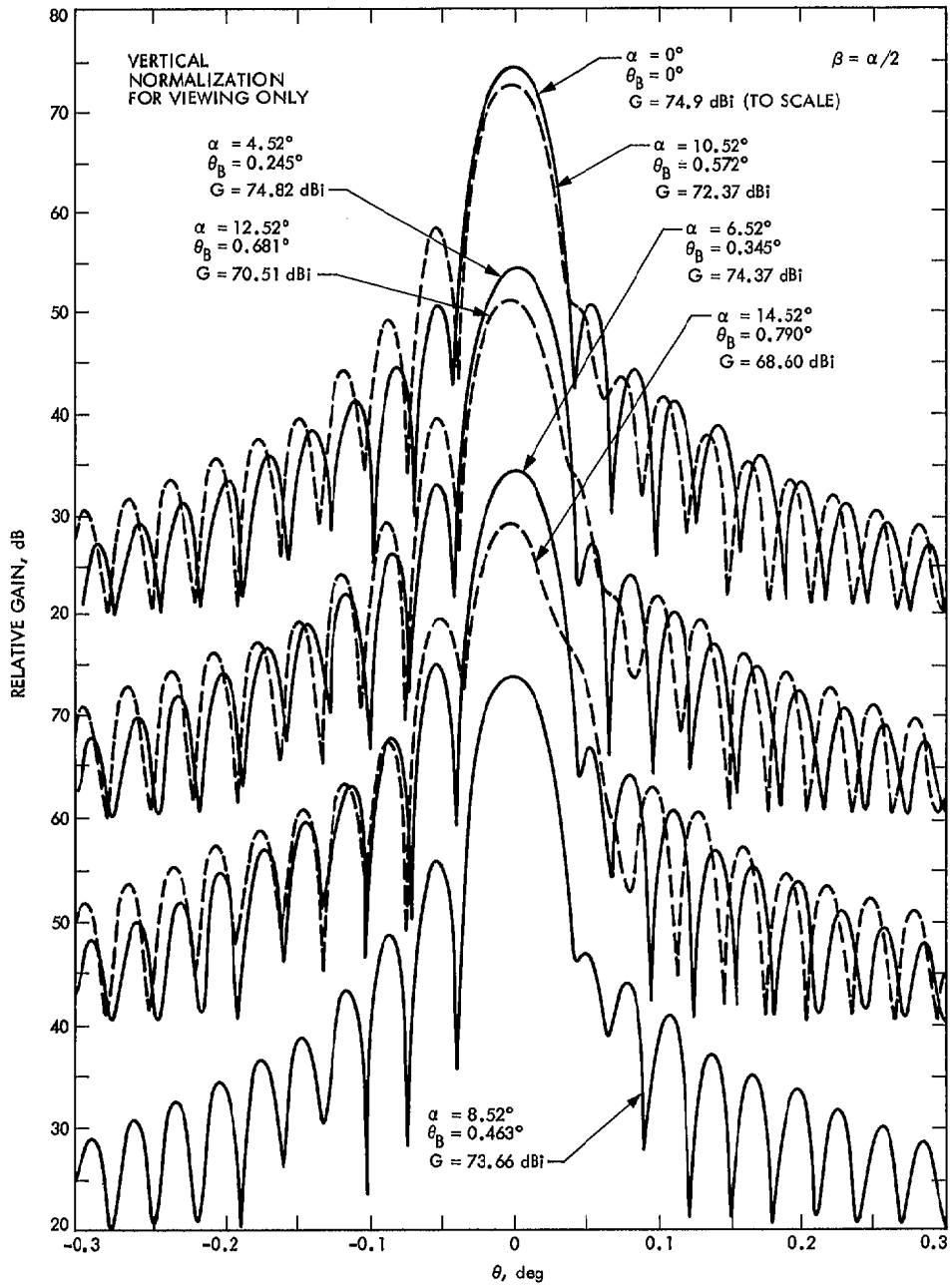


Fig. 13. Far-field gain patterns of the Cassegrainian antenna with  $\beta = \alpha/2$

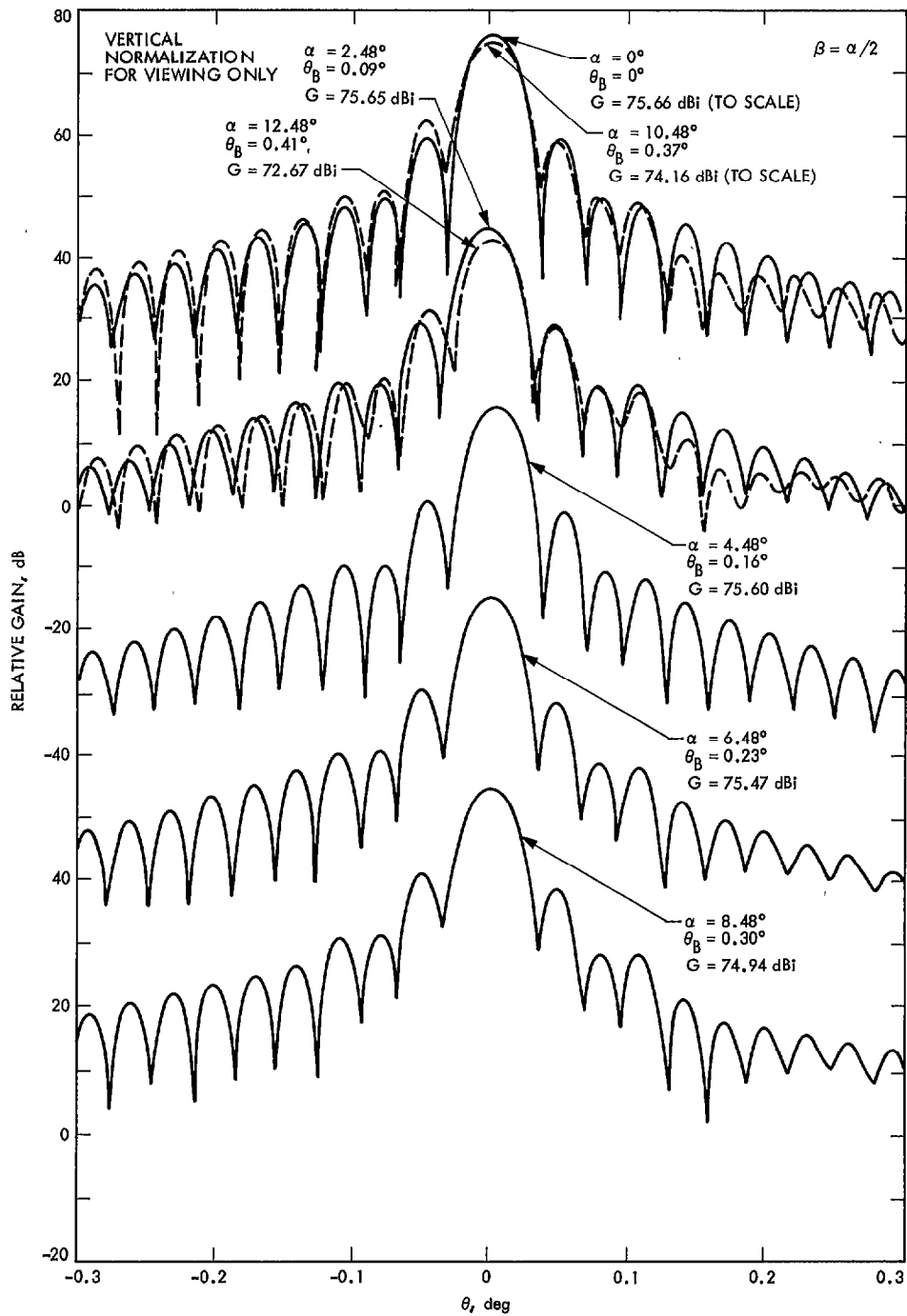


Fig. 14. Far-field gain patterns of the dual-shaped (with vertex plate) antenna with  $\beta = \alpha/2$

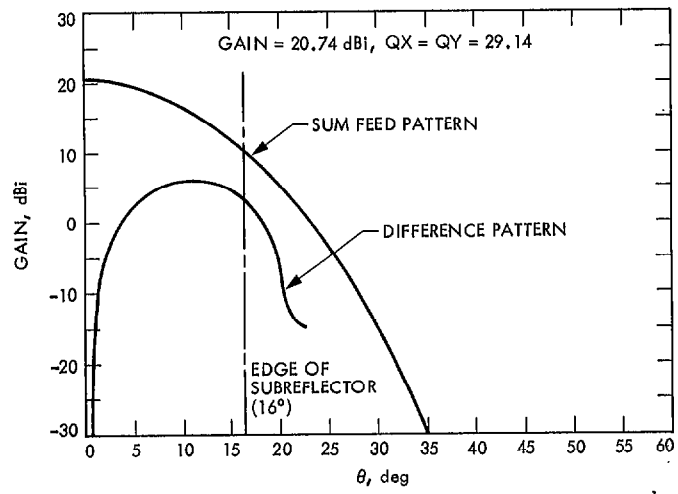


Fig. 15. Feed horn radiation patterns

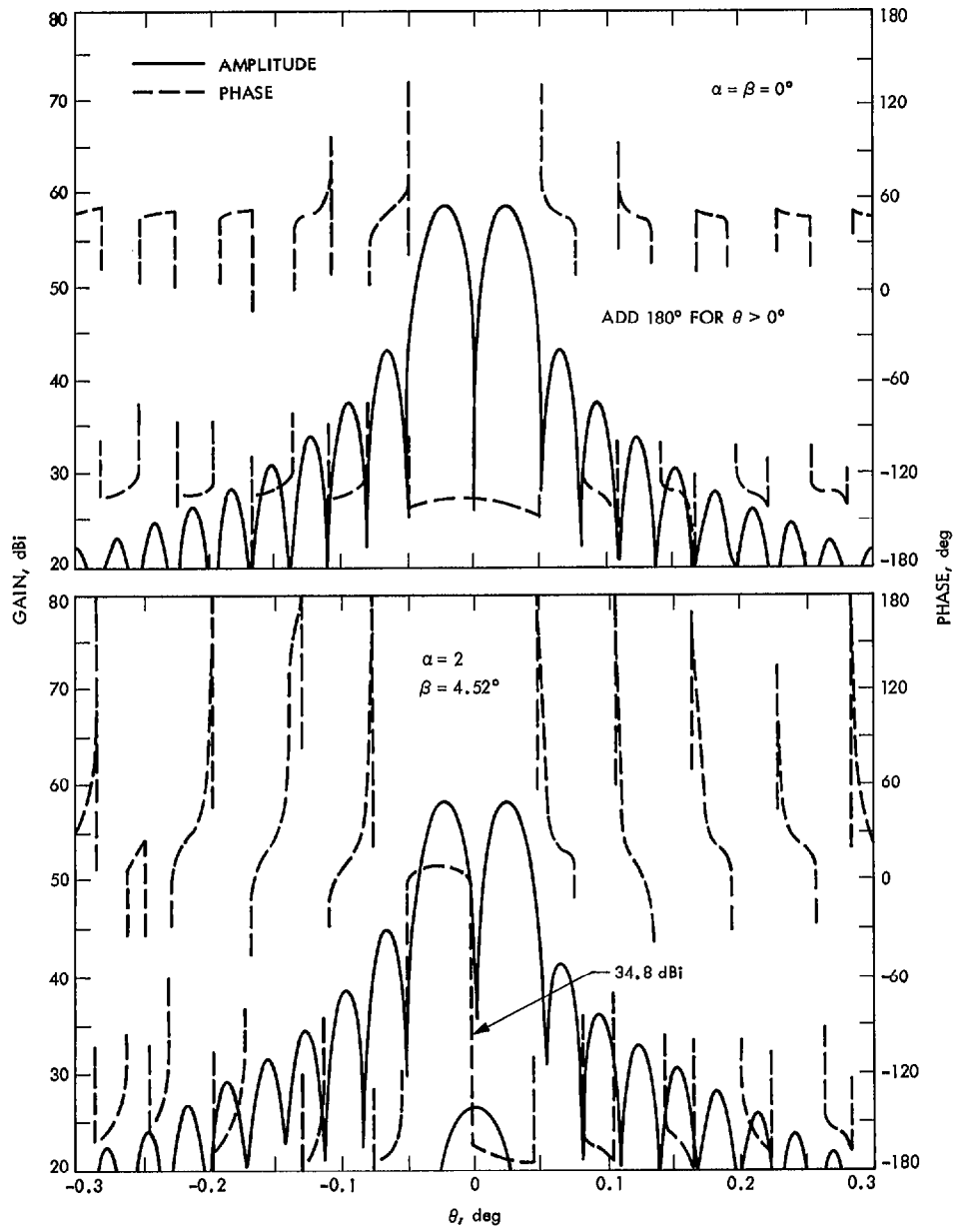


Fig. 16. Difference pattern of the Cassegrainian antenna

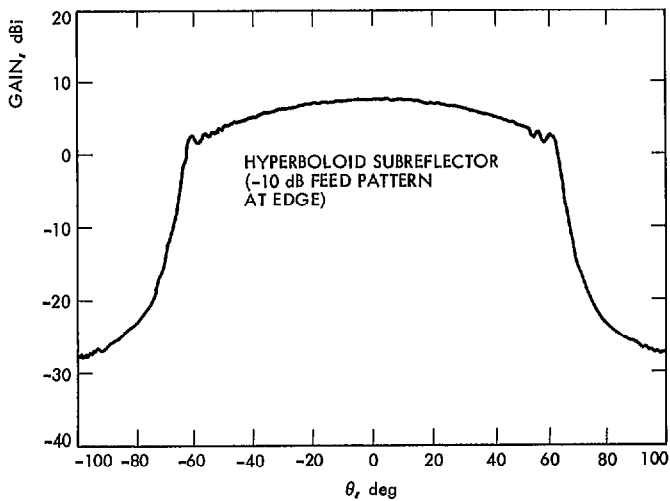
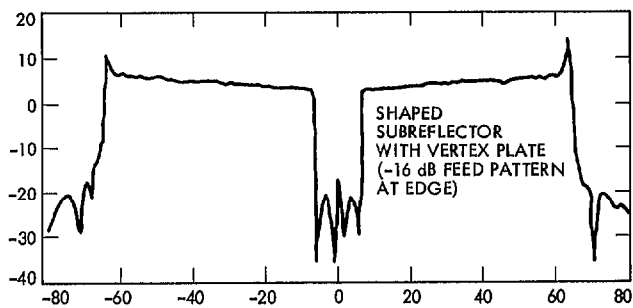
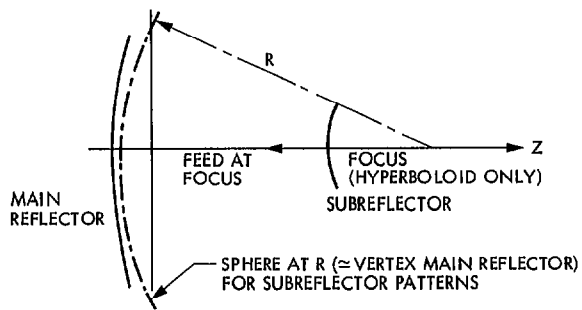


Fig. 17. Subreflector scatter patterns

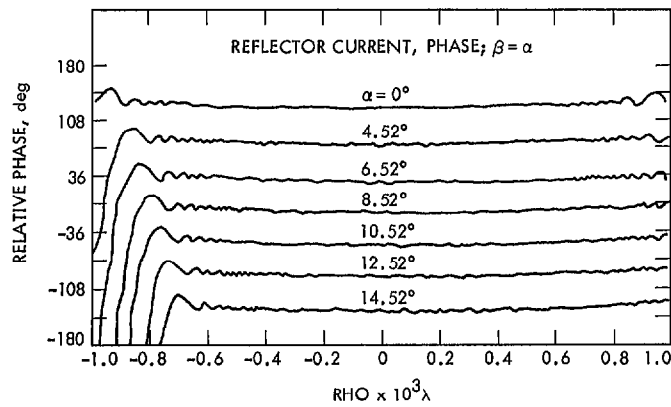
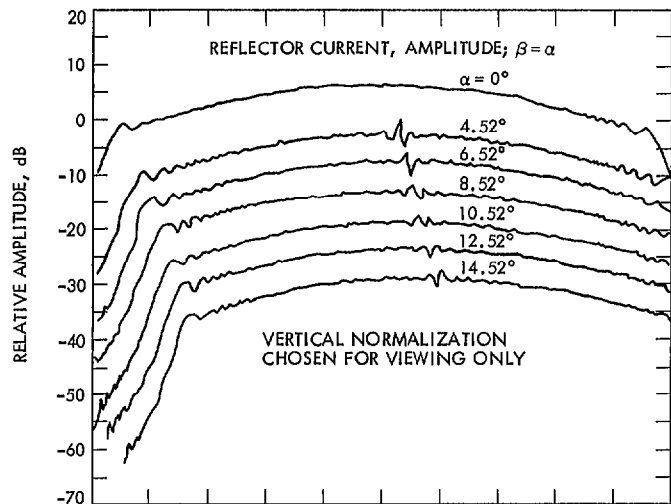


Fig. 18. Aperture current distributions of the Cassegrainian antenna for  $\beta = \alpha$

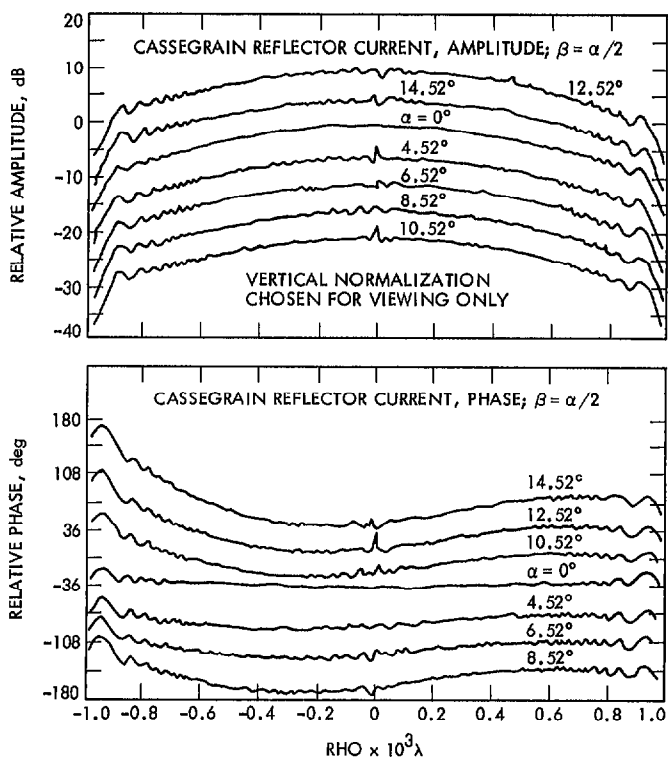


Fig. 19. Aperture current distributions of the Cassegrainian antenna for  $\beta = \alpha/2$

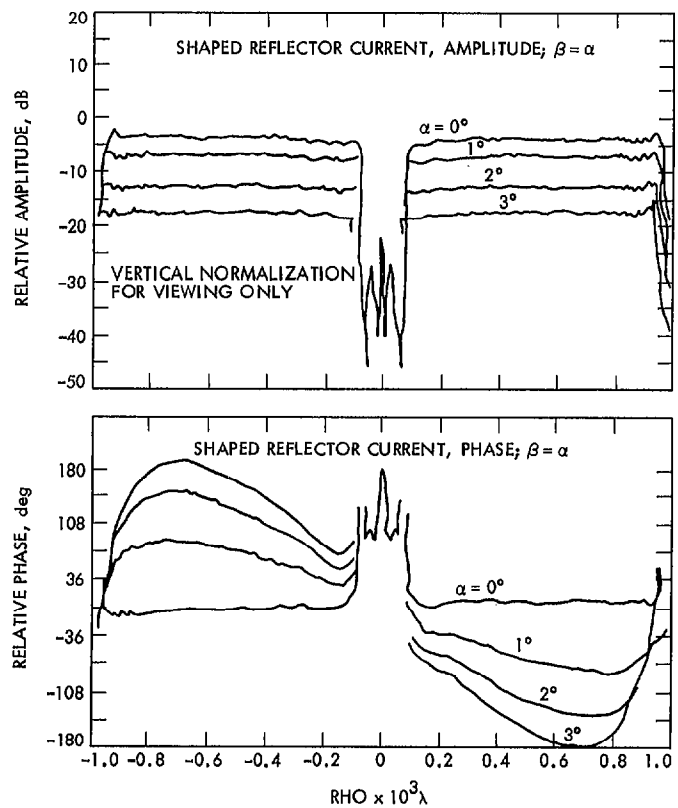


Fig. 20. Aperture current distribution of the shaped antenna for  $\beta = \alpha$

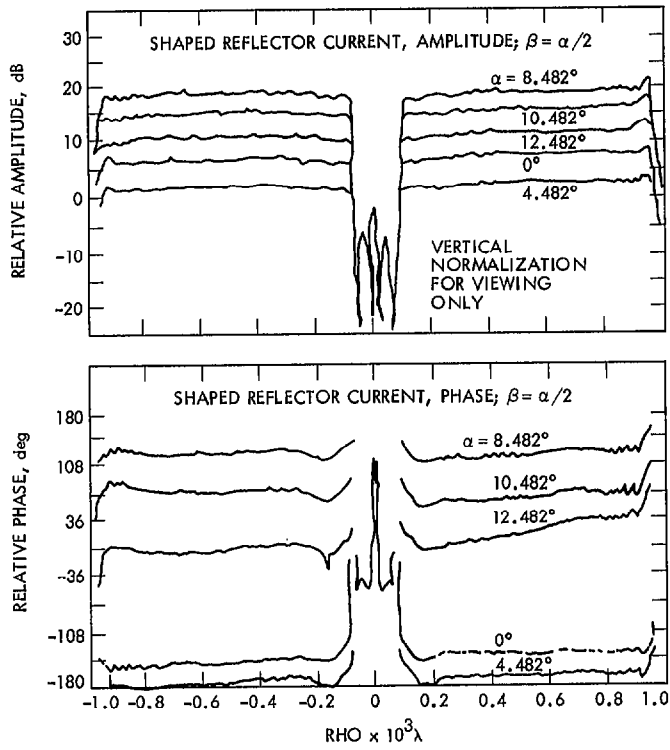


Fig. 21. Aperture current distribution of the shaped antenna for  $\beta = \alpha/2$

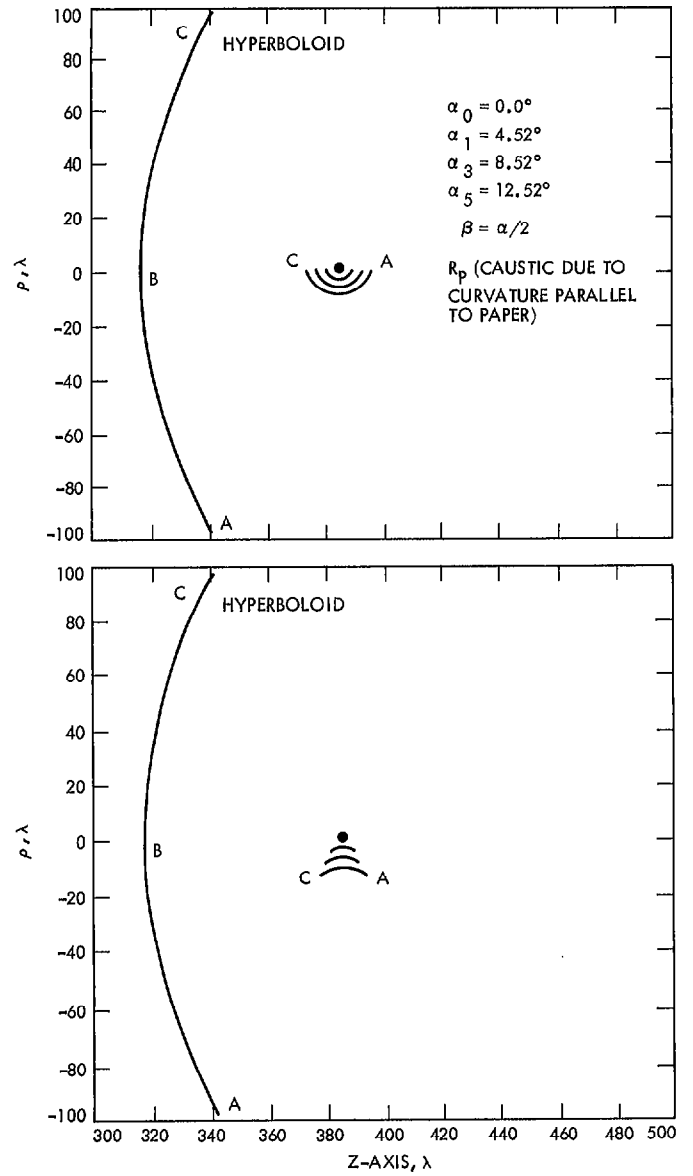


Fig. 22. Caustic surfaces of field scatter from the subreflector of the Cassegrainian antenna

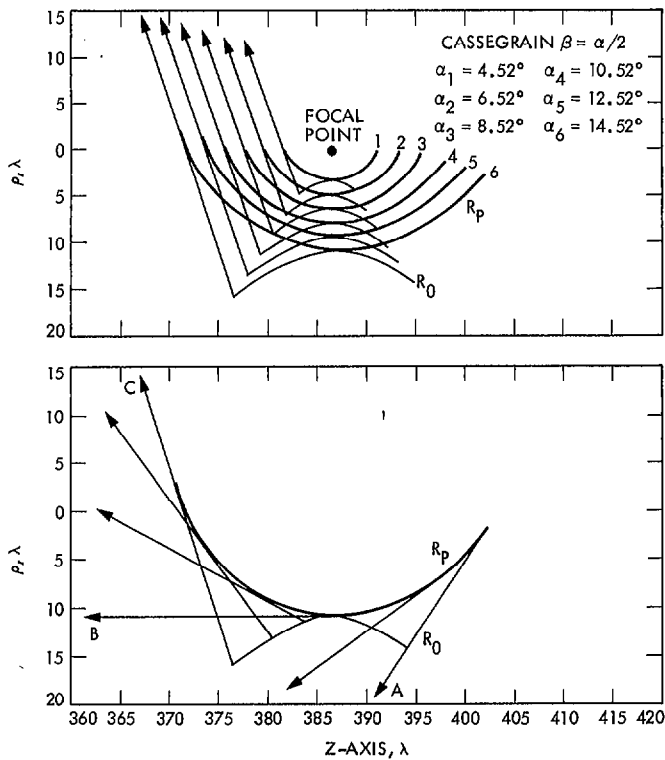


Fig. 23. Caustic surfaces of field scatter from the subreflector of the Cassegrainian antenna, expanded scale

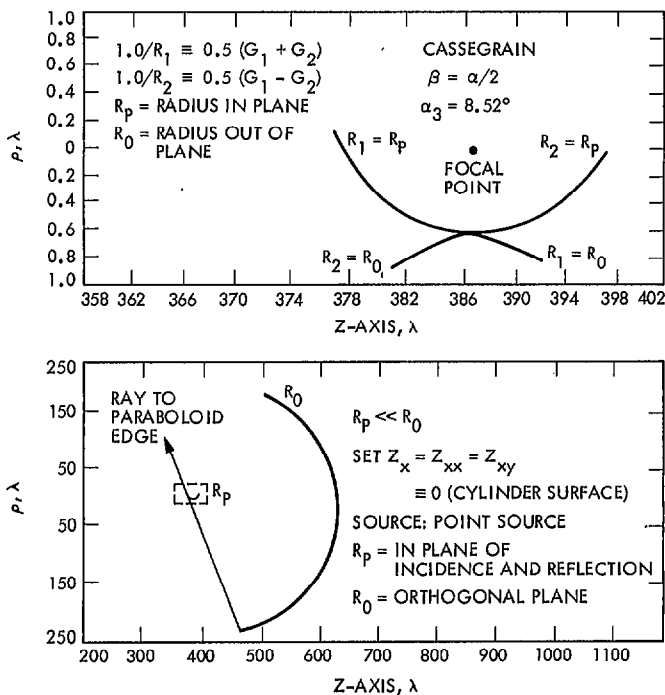


Fig. 24. Caustic surfaces of field scatter from the subreflector of the Cassegrainian antenna where set  $Z_x = 0$

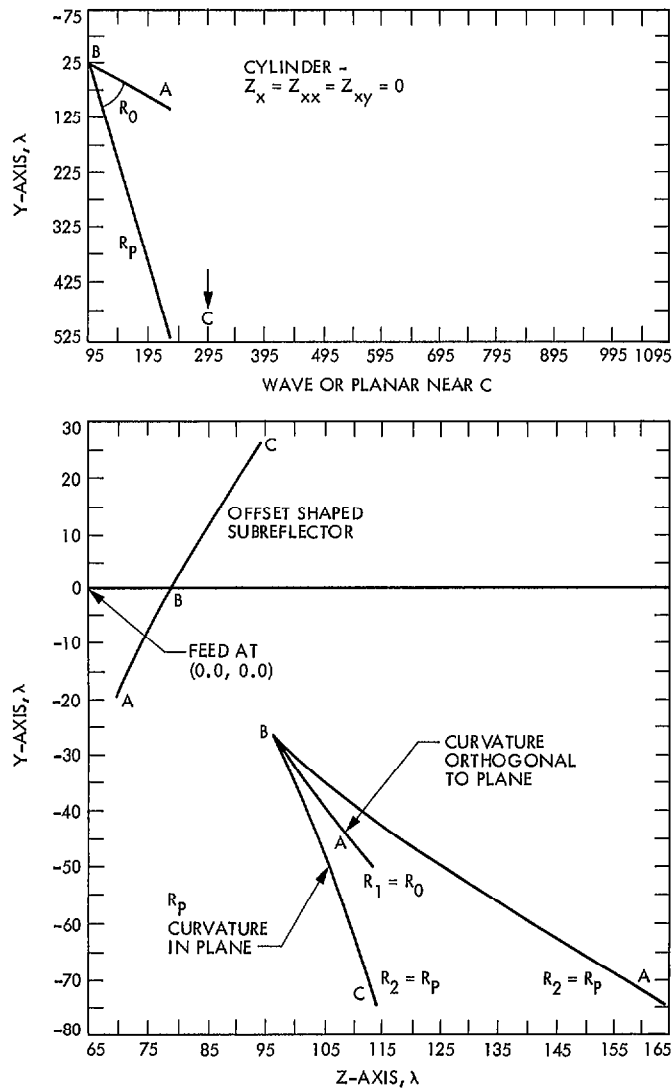


Fig. 25. Caustic surfaces of field scatter from the subreflector of the dual-offset shaped reflectors

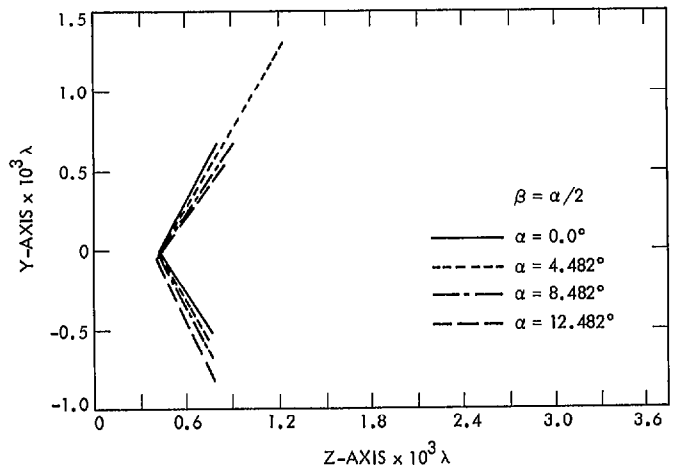
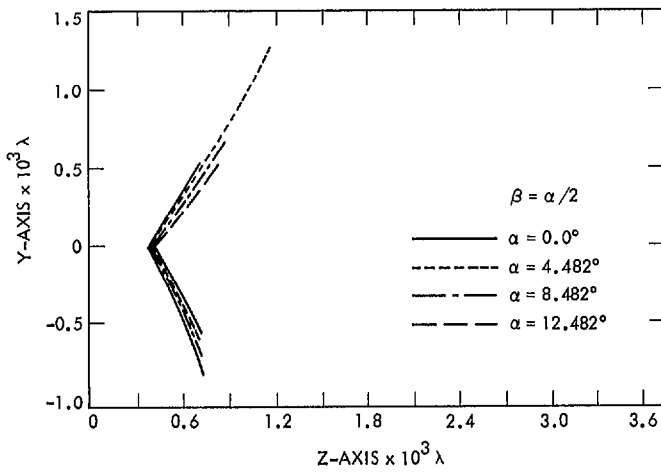
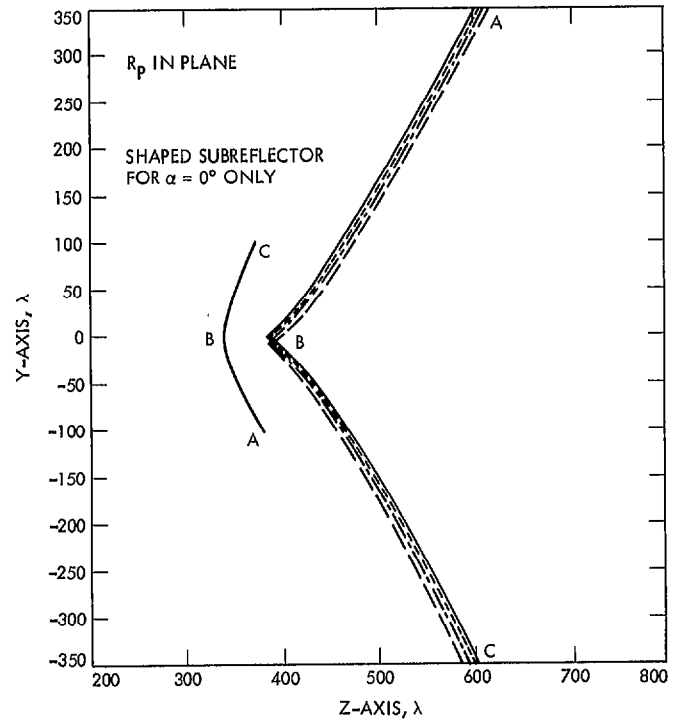
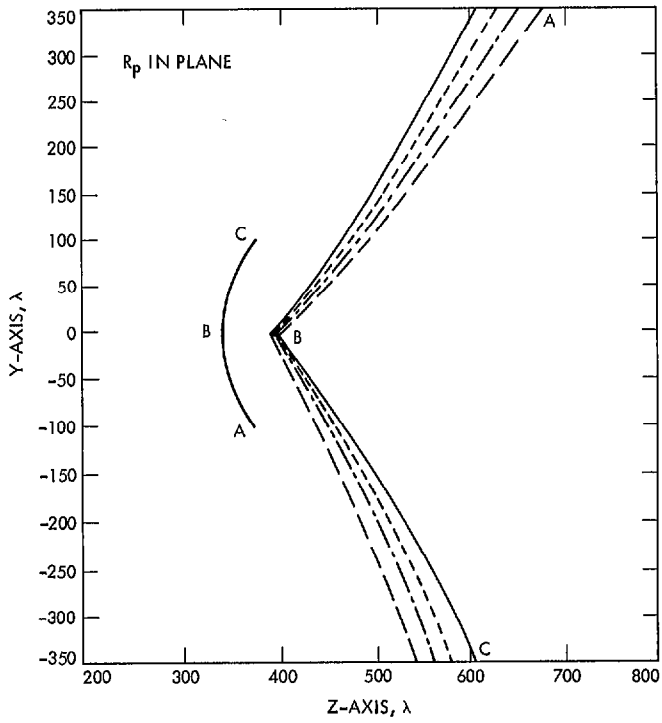


Fig. 26. The  $R_p$  caustics (parallel to plane) with respect to shaped subreflector (70-m)

Fig. 27. The  $R_p$  caustics (parallel to plane) with respect to shaped main reflector (70-m)

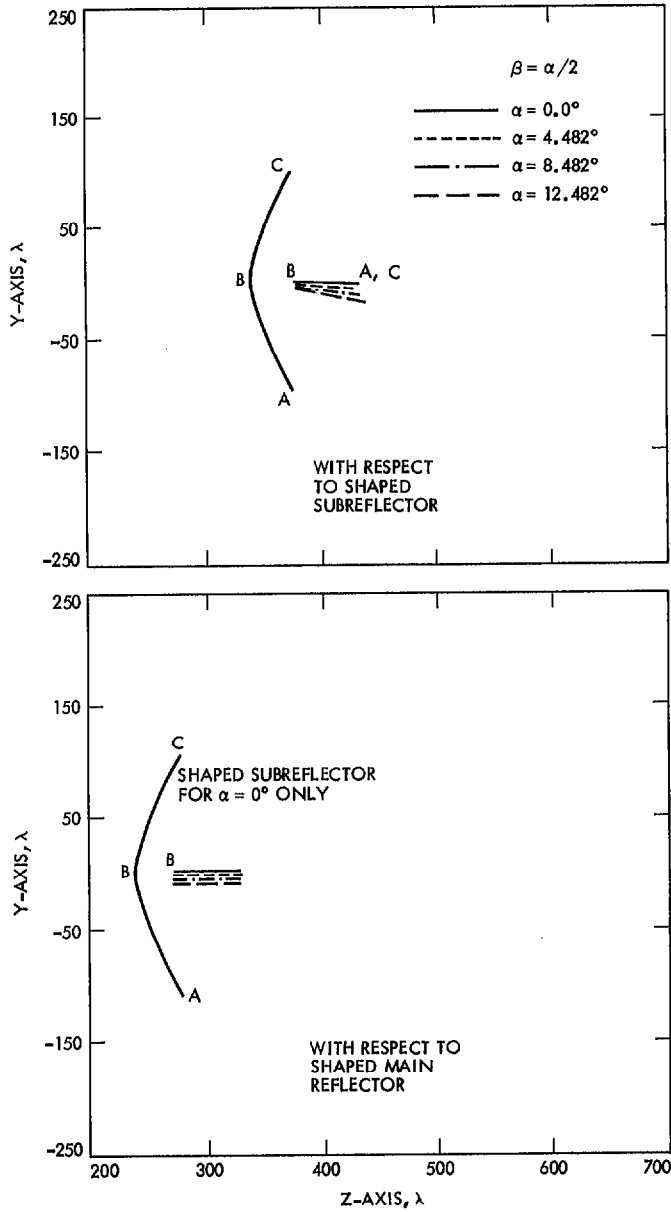


Fig. 28. The  $R_0$  caustics (orthogonal to plane) with respect to shaped subreflector and shaped main reflector (70-m)

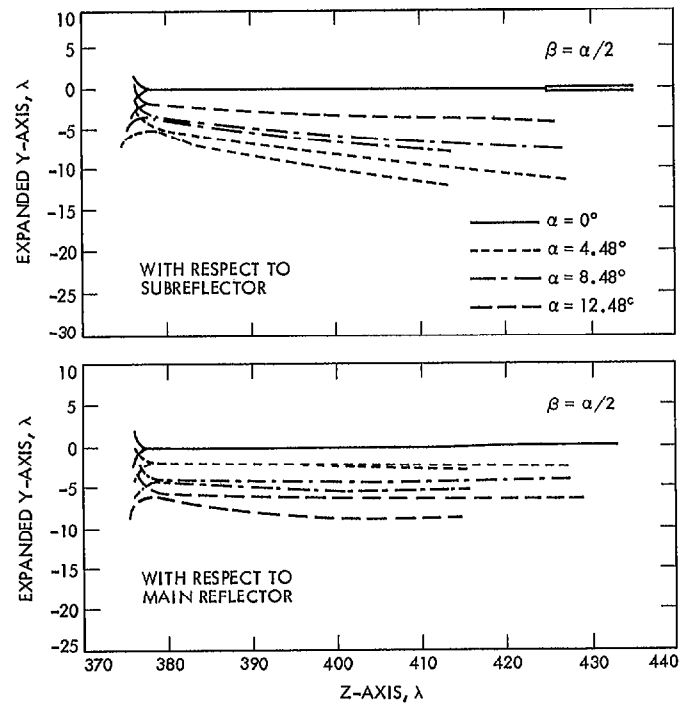


Fig. 29. The  $R_0$  caustics (orthogonal to plane) with respect to shaped subreflector and shaped main reflector (70-m), expanded scale

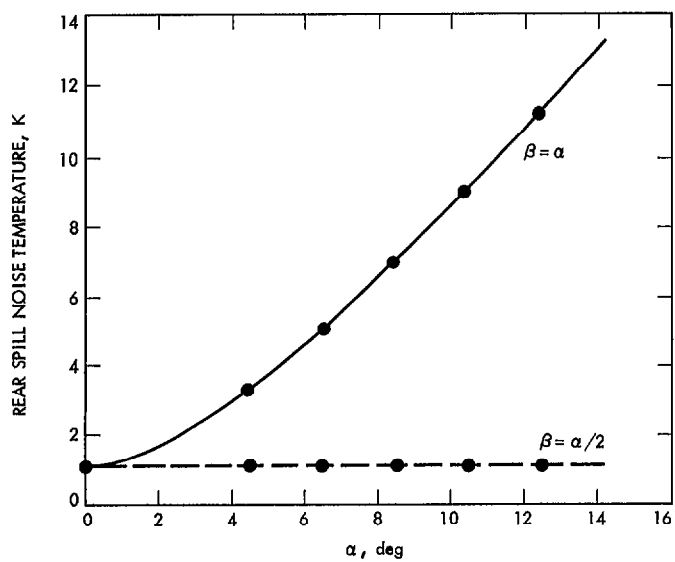
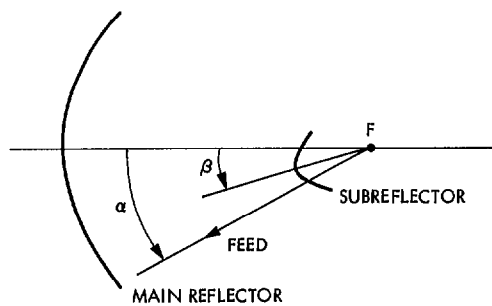


Fig. 30. The 70-m Cassegrainian near spillover noise temperature

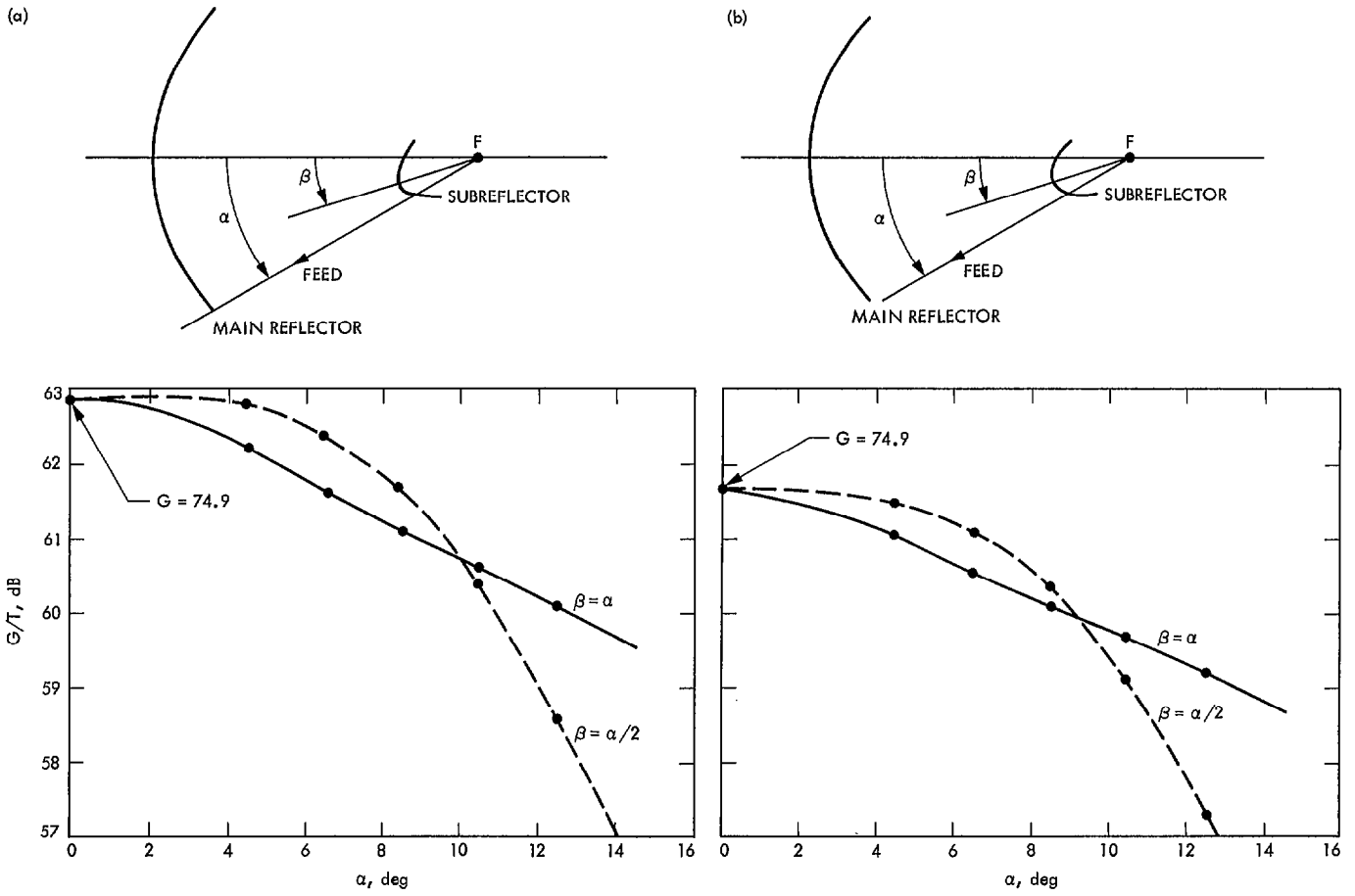


Fig. 31. The 70-m Cassegrainian  $G/T$  where  $T_{\text{system}} - T_{\text{antenna noise}}$  equals (a) 14.6 K and (b) 20 K